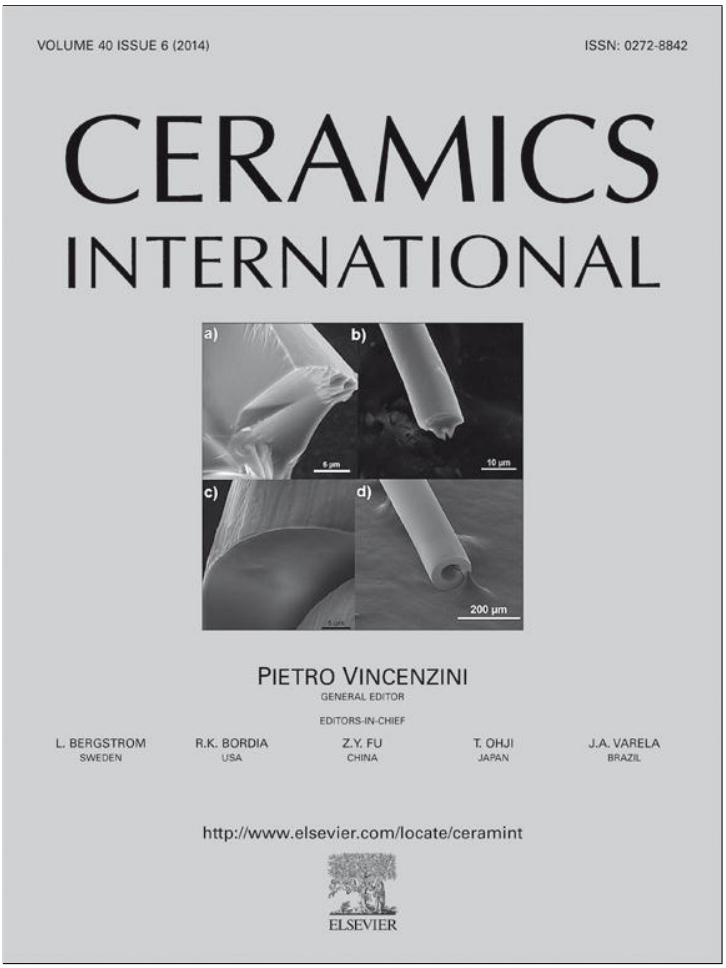

Available online at www.sciencedirect.com

ScienceDirect

Ceramics International 40 (2014) 7965–7970

CERAMICS INTERNATIONAL

www.elsevier.com/locate/ceramint

ZnO photoanodes with different morphologies grown by electrochemical deposition and their dye-sensitized solar cell properties

Min Zi[a], Min Zhu[a], Ling Chen[a], Haoming Wei[c], Xiaopeng Yang[a], Bingqiang Cao[a,b,*]

[a]School of Material Science and Engineering, Key Lab of Inorganic Functional Material in Universities of Shandong, University of Jinan, Jinan 250022, China
[b]Shandong Provincial Key Lab of Preparation and Measurement of Building Materials, University of Jinan, Jinan 250022, China
[c]Institut für Experimentelle Physik II, Universität Leipzig, Linnéstraße 5, D-04103 Leipzig, Germany

Received 24 November 2013; received in revised form 27 December 2013; accepted 27 December 2013
Available online 8 January 2014

Abstract

In this article, we grew zinc oxide (ZnO) samples with different morphologies, e.g. film, nanowire and nanosheet, with electrochemical deposition (ECD) by controlling the precursor concentration and the growth mechanism was also discussed. The morphology influence on the photovoltaic conversion efficiency of the dye-sensitized solar cells (DSSC) assembled with different ZnO photoanodes was investigated by measuring current density–voltage (*J–V*) curve, quantum efficiency (QE) spectrum and electrochemical impedance spectrum (EIS). It was found that the DSSC constructed with ZnO nanowire array as photoanode can absorb more dye, improve the photon utilization rate and provide rapid collection channels for the photoexcited carriers. Therefore, the photovoltaic conversion efficiency of ZnO nanowire DSSC was improved.

Keywords: D. ZnO; Electrochemical deposition; Morphology of photoanodes; Dye-sensitized solar cell

1. Introduction

With economic development and the rapid growth of population, there came out more violent conflicts among energy, environment and population. The global focus has switched to developing green renewable energy, among which the most promising one is solar energy. The commercial silicon solar cells with high production costs as well as a more complicated preparation process has limited its efficiency and a wide range of civil application [1,2]. As a consequence, an alternative way for solar cell [3,4] is to develop new materials and assembling methods for cheap solar cells. As one of the third-generation solar cells, dye-sensitized solar cell (DSSC) has attained wide attention due to its low production cost and flexible production methods. In the dye-sensitized solar cells, the potoanodes play a vital role in the conversion process of light into electrical energy. ZnO is a kind of n-type semiconductor with a direct band gap of 3.37 eV and has been found to have the similar energy band structure and physical properties with TiO_2, which has acted as the frequently used material for DSSC photoanodes, while its electron mobility is higher by 2–3 orders of magnitude [5] which will help improve the efficiency of photo-generated electron transfer and reduce the electron recombination probability [6]. Therefore, ZnO is expected to exhibit faster electron transport with reducing the loss of recombination.

It is reported that ZnO nanostructure shows a variety of different morphologies, such as nanoparticle [7], nanowire [8], nanosheet [9], nanoflower [10] and nano-wall [11], and it has demonstrated many interesting applications for various types of optoelectronic devices. The preparation methods of ZnO nanostructures include hydrothermal growth [12], sputtering [13], spray pyrolysis [14], sol–gel [15], chemical vapor deposition [16] and electrochemical deposition (ECD) [17]. In the past years, different ZnO nanostructures grown with ECD was adopted as photoanodes in DSSCs. Wang et al. [18] has proved the dyed ZnO film showed well-structured photovoltage response in the visible range which made it potentially applicable in DSSCs. One dimensional ZnO nanostructures based DSSC has been extensively investigated because the direct electrical pathways for photocarriers and big surface area for more dye could enhance the cell efficiency [19]. Hsu et al. fabricated a DSSC with nanorods prepared with vapor deposition

*Corresponding author at: Shandong Provincial Key Lab of Preparation and Measurement of Building Materials, University of Jinan, Jinan 250022, China. Tel.: +86 531 89736292; fax: +86 531 87974453.
E-mail address: mse_caobq@ujn.edu.cn (B. Cao).

0272-8842/$ - see front matter © 2014 Elsevier Ltd and Techna Group S.r.l. All rights reserved.
http://dx.doi.org/10.1016/j.ceramint.2013.12.146

method achieving a light-harvesting efficiency of 0.22% [20]. Meng et al. grew ZnO nanorod/nanoparticle composite anode by surface attachment and electrochemical deposition and achieved a light-harvesting efficiency of 1.66% [21]. Although the electrochemical deposition is widely used in the synthesis of ZnO due to its mild reaction conditions, the controlled growth of a variety of ZnO nanostructures for device applications remains to be an open challenge.

In this paper, we grew ZnO samples showing three different morphologies, e.g. film, nanowire and nanosheet, by controlling the precursor concentration on the FTO-glass with ECD method. Then DSSCs are constructed with ZnO of different morphologies as photoanodes. Finally, the influence of the different morphologies of ZnO nanostructures on the DSSC performance was investigated by measuring the cell current density–voltage curve (*J–V*), quantum efficiency (QE) and electrochemical impedance spectrum. It was demonstrated that the cell efficiency of the DSSC assembled with ZnO nanowires was much higher than that of ZnO film and nanosheets.

2. Experimental section

2.1. ZnO nanostructure growth and DSSC assembly

In our work, three-electrode electrochemical deposition is applied for the synthesis of ZnO samples. The FTO-glass substrate acts as the working electrode, a zinc plate plays as a counter electrode, and saturated Ag/AgCl electrode is chosen as a reference electrode. $Zn(NO_3)_2 \cdot 6H_2O$ of different concentrations are selected as electrolyte. Prepared samples are annealed at 500 °C for 30 min through a rapid annealing process.

To fabricate DSSCs, the dyed ZnO photoanodes were limited to about $0.6 \times 0.6\ cm^2$ by removing extra with a blade. The annealed ZnO samples were immersed in 0.5 mM $(Bu_4N)_2$[Ru(4,4′-(COOH)-2,2,-bipyridine)$_2$(NCS)$_2$] (N719 dye) ethanol solution for 24 h to absorb dye. A 25 μm thick hot-melt sealing gasket (Surlyn1702) frame was sandwiched between the dye-sensitized electrode and platinized FTO counter electrode. The sandwiched structures were symmetrically clamped with two binder clips to keep the pressure balance. They were heated in drying baker at 90 °C for 3 min, and then removed the binder clips after cooling to the room temperature. A solution consisting of 0.05 M I_2, 0.5 M LiI, 0.5 M 4-tertbutylpyridine and 0.3 M DMPII in acetonitrile was introduced into the cell by vacuum backfilling [22]. The opening was immediately sealed with the cover glass.

2.2. Sample characterizations

Morphology studies of grown ZnO nanostructures have been performed with a field emission scanning electron microscope (FE-SEM, Quanta 250, FEI). X-ray diffraction (XRD, D8-Advance, Bruker) was used to examine the crystal structure of the ZnO photoanodes. The diffused reflectance and transmittance spectra were measured with UV–vis–NIR spectrophotometer (UV-3600, Shimadzu) equipped with an integrating sphere. Photovoltaic measurements were recorded employing a Keithley 2612A source/meter under simulated sunlight (AM 1.5, 100 mW cm^{-2}, San-Ei). The QE measurement was carried out using a QEX 10 system (PV Measurement). A reference Si photodiode calibrated for spectral response was used for the monochromatic power–density calibration. Electrochemical impedance spectra (EIS) of fully assembled DSSC was measured in the dark at the cell open-circuit voltage applied forward bias using a Zahner Zennium electrochemical workstation. The spectra were scanned in a frequency range of 1–100 mHz with an perturbation voltage of 10 mV.

3. Results and discussion

3.1. Structural analysis of ZnO nanostructures

Fig. 1 shows the SEM images of ZnO samples prepared by electrochemical deposition when the precursor concentration is different. The other ECD conditions were all set the same, e.g. growth time of 1 h, deposition temperature of 80 °C, and applied current density of 0.3 mA cm^{-2}. It was found that ZnO samples with different morphologies can be grown by varying the concentration of zinc nitrate precursor. When the precursor concentration was 0.05 M, quasi-aligned ZnO nanowires can be grown on the FTO-glass substrates, as shown in Fig. 1(a) and (b). When the concentration was increased to 0.1 M, dense ZnO film was observed, as shown in Fig. 1(c). While, interconnected two-dimensional ZnO nanosheets were obtained, as shown in Fig. 1(d), when the precursor concentration was further increased to 0.3 M.

Fig. 2 shows the XRD patterns of three ZnO samples with different morphologies as shown in Fig. 1. It is shown that, compared with the standard PDF card (JCPDS 36-1451), all the peaks can be ascribed to ZnO characteristic diffraction peaks with a hexagonal wurtzite structure except for the weak diffraction peaks with asterisks from the FTO-glass substrates. The (002) diffraction peak of ZnO nanowires is of the maximum intensity, indicating that ZnO nanowire growth orientation of the *c*-axis is obvious. The diffraction peaks of ZnO nanosheets showed weak intensity, while the underlying FTO film has stronger diffraction peaks as can be seen in Fig. 1(d). This indicates ZnO nanosheets were relatively sparse and part of FTO is uncovered with nanosheets. The XRD peaks of the ZnO film almost show similar intensity, indicating the film is composed of nanocrystals with random orientation along the three typical directions of (100), (101) and (001), which is consistent with the SEM image of Fig. 1(c).

For electrochemical deposition, ZnO nanostructures are synthesized based on the following chemical reactions [23]:

$$Zn(NO_3)_2 \rightarrow Zn^{2+} + 2NO_3^-$$

$$NO_3^- + H_2O + 2e^- \rightarrow NO_2^- + 2OH^-$$

$$Zn^{2+} + 2OH^- \rightarrow Zn(OH)_2$$

$$Zn(OH)_2 \rightarrow ZnO + H_2O$$

Reduction of the nitrate (NO_3^- to NO_2^-) in mild acid solution of Zn^{2+}, which results in an increase of the pH value near the electrode surface is crucial [24]. With increasing concentration of OH^-, $Zn(OH)_2$ will form and deposit on

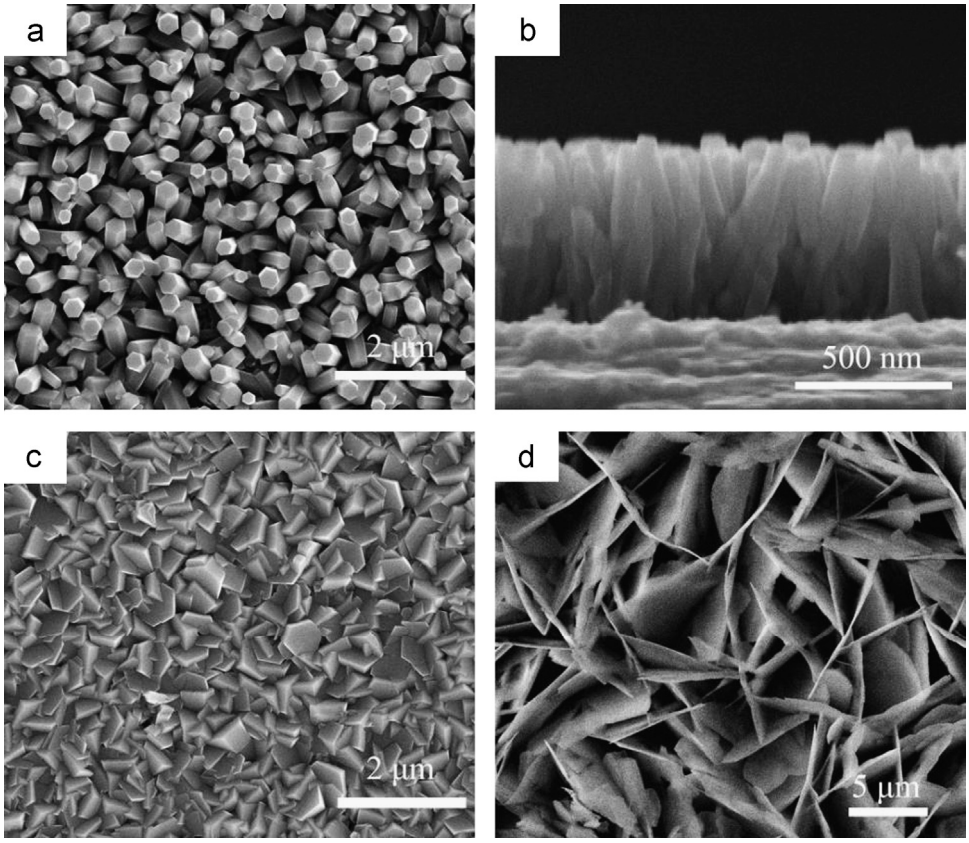

Fig. 1. SEM images of ZnO nanostructures grown by ECD showing different morphologies, (a) nanowire, (b) cross-sectional SEM image of nanowire, (c) film, and (d) nanosheets.

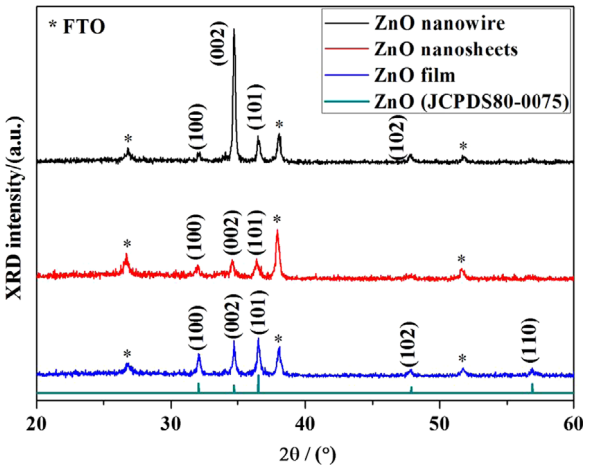

Fig. 2. XRD patterns of different ZnO samples grown on FTO-glass substrate. Vertical lines are PDF card (JCPDS 36-1451) of ZnO.

the cathode electrode. The deposited $Zn(OH)_2$ will subsequently be decomposed and ZnO grow on the substrate at a moderate high temperature of 80 °C. In fact, the nucleation and growth process of the ZnO are controlled by several ECD parameters, including cathodic potentials, electrolyte, and cathodic substrates. In our work, all ECD parameters are fixed except the precursor concentration. Moreover, it is well known that ZnO is a polar crystal and produces positively Zn^{2+}-terminated (0001) and negatively O^{2-}-terminated $(000-1)$ polar surfaces, which induces a net dipole moment along the *c*-axis [25]. Generally, their growth directions are perpendicular to high surface energy planes [26]. The surface energy of the polar (0001) planes is higher than that of nonpolar $(01-10)$ and $(2-1-10)$ planes. So, preferential growth along the *c*-axis is energetically favorable [27]. In other words, (0001)-oriented ZnO nuclei will grow faster.

When the concentration of the precursor solution is low, the (001)-oriented ZnO nuclei grow rapidly along the *c*-axis direction in thermodynamic equilibrium. As a result, the ZnO sample obtained at precursor of 0.05 M was constituted by the (001)-oriented ZnO nanowires, as shown in Fig. 1(a and b). When the concentration of the precursor was increased, the growth rate ratio of ZnO along the *c*-axis and the *a*-axis direction was changed. Thus the ZnO film with random oriented crystallites is formed. However, if the precursor solution is too high, the formation of the two-dimensional ZnO nanosheets is another completely different growth behavior from ZnO nanowire array or film. Illy et al. [28] and Zarebska et al. [29] also observed two-dimensional ZnO nanosheets in the ECD process by using zinc metal sheet as the substrate. The growth of such two-dimensional nanosheets was attributed to the minor surface energy difference between

one-dimensional and two-dimensional crystal growth modes under suitable conditions. However, in this experiment, we believe that this unique two-dimensional ZnO nanosheets growth is a rapid non-equilibrium growth mode [30,31] caused by the high concentration of precursor solution.

3.2. Optical properties of different photoanodes

Fig. 3(a) shows the optical reflectance spectra of different ZnO samples without dye and Fig. 3(b) is the transmittance spectra of the corresponding samples sensitized with N719 dye for 24 h. From Fig. 3(a) we can see that in the visible range the reflectivity of nanowires, nanosheets and film decreased in turn. It means ZnO nanowire array reflects light more effectively and, therefore, can capture more sunlight after dye adsorption. Accordingly, the transmittance of ZnO nanowires in Fig. 3(b) is the lowest. The reflection spectra together with the absorption data indicate that the absorption of ZnO nanowires is relatively strong after absorbing the dye in comparison with ZnO nanosheet and film samples. The significant absorption peak at the wavelength of 530 nm in Fig. 3(b) is the typical absorption of N719 dye. So, the ZnO nanowire-based solar cells could be expected to be of more dye loading and light harvesting.

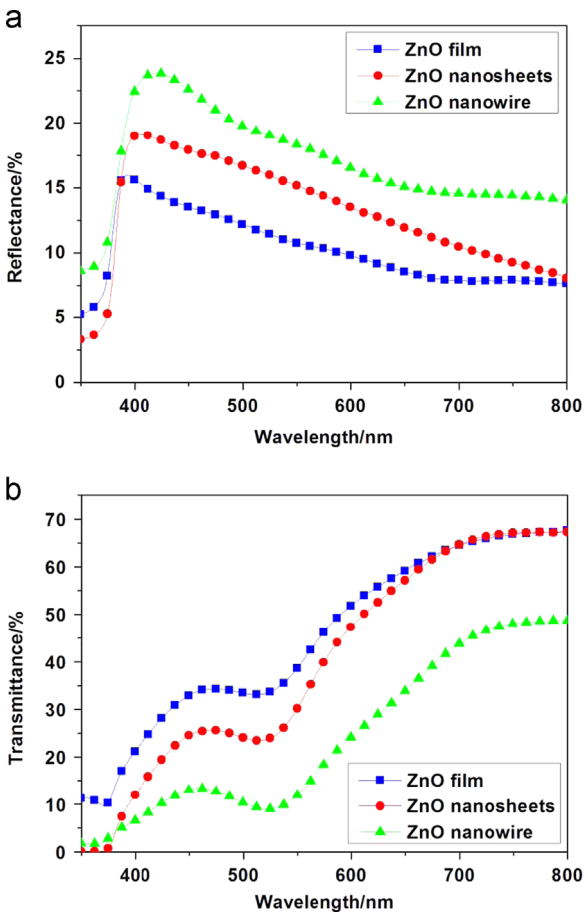

Fig. 3. (a) The reflectance spectra of different ZnO samples without dye, (b) the corresponding transmittance spectra of ZnO samples after sensitization with N719 dye.

3.3. The performance of different DSSC

The current–voltage characteristic curves of DSSCs assembled with three different ZnO anodes under simulated AM 1.5 light are shown in Fig. 4(a) and the corresponding open circuit voltage (V_{OC}), short circuit current density (J_{SC}), fill factor (FF) and the photovoltaic conversion efficiency (η) are shown in Table 1. As can be seen from the above, with the same cell assembly process, these four characteristic parameters of ZnO nanowire DSSC are the highest, followed by ZnO nanosheet cell, and the film cell is the minimum. Theoretically, the DSSC open circuit voltage (V_{OC}) is the difference between the quasi-Fermi level (E_F) of semiconductor anode and the Nernst redox potential (E_N) of the electrolyte, e.g. $V_{OC}=E_F-E_N$.

However, there exists shunt resistance in the solar cell. For DSSCs prepared with different ZnO anodes, the shunt resistance increases with the increasing of ZnO anode surface area because the available area between ZnO anode and the electrolyte becomes large. The shunt resistance can reduce the cell leakage current and also increase the open-circuit voltage. So, the nanowire-based DSSC exhibits the biggest J_{sc} and V_{oc}. In DSSC, series resistor (R_S) also exists and, when the current is not zero, there will be a voltage drop (IR_S) in the output terminal of the cell. Therefore, the influence of series resistance on the filling factor is very significant. One-dimensional single crystal ZnO nanowire provides a more direct electronic transmission channel, and the series resistance is

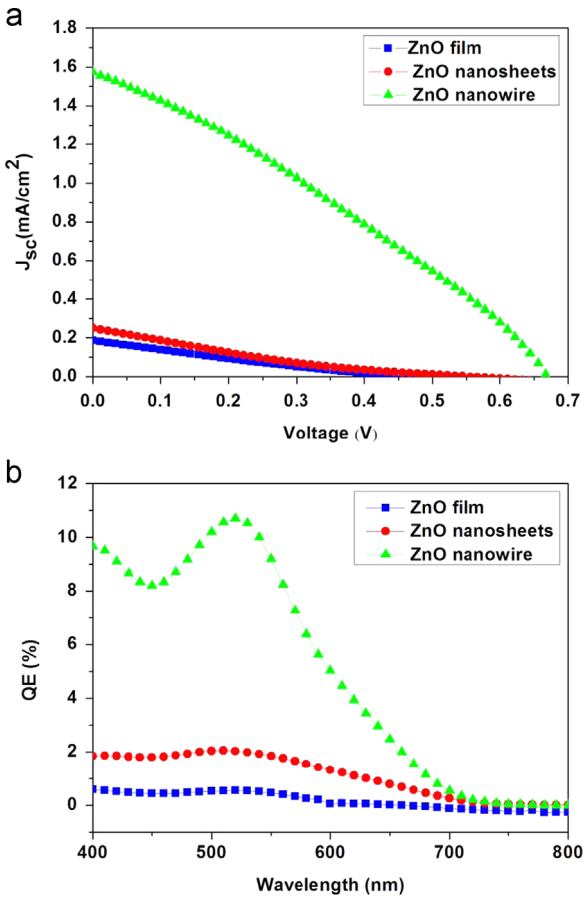

Fig. 4. Photovoltaic performance of DSSCs fabricated using different ZnO photoanodes: (a) current density–voltage (J–V) curve; (b) QE spectrum.

Table 1
Photovoltaic performance data of different ZnO DSSCs derived from Fig. 4(a).

ZnO samples	V_{OC} (V)	J_{SC} (mA cm^{-2})	FF (%)	η (%)
Film	0.4495	0.1855	17.88	0.018
Nanosheet	0.5536	0.2501	22.01	0.025
Nanowire	0.6688	1.5743	30.12	0.320

relatively small during electron transfer process. The resulting voltage drop across the solar cell is small and, therefore, the FF of ZnO nanowires DSSC is also the largest.

Fig. 4(b) shows the corresponding QE spectrum of three ZnO DSSCs shown in Fig. 4(a). The maximum of QE in the visible region is located at about 530 nm. This is approximately consistent with the expected maximum based on the accompanying absorption spectrum for the N719 dye (with local maxima at 390 and 535 nm), both corresponding to a metal-to-ligand charge transfer transition. The quantum efficiency of ZnO nanowires DSSC is much larger than the others, which is the reason for larger short-circuit current density of ZnO nanowires DSSC. This is mainly due to the different morphologies of the ZnO photoanodes.

The specific surface area of ZnO nanowires and nanosheets are greater than that of the dense ZnO film and they are able to absorb more dye. Meanwhile, as the sample surface of nanowires and nanosheets are rough, the diffuse light scattering can improve the utilization of photons. Therefore, the quantum efficiency at the same wavelength of ZnO nanowire and nanosheet cells show higher values and the photocurrent density is bigger. Moreover, the QE of ZnO nanowires DSSC is still much higher than the corresponding nanosheets DSSC. The one-dimensional ZnO nanowires provide direct pathways which can reduce the possibility of charge recombination during interparticle percolation. So, the photo-generated carriers transport more easily. The higher short-circuit current density is the main reason for the nanowire DSSC efficiency improvement.

To further study the transport process of photo-carriers in solar cells, the EIS spectrum of the three different DSSCs were measured, as shown in Fig. 5. The semicircular curve shows the dark reaction impedance caused by electron transport in ZnO and electron transmission from the ZnO conduction band to the I_3^- ions in the electrolyte [32]. As can be seen from Fig. 5, the radius of the semicircular curve of ZnO film and ZnO nanosheet cells are much larger than that of ZnO nanowire cell, which indicates that the impedances of ZnO film and nanosheet DSSCs are much larger than that of the ZnO nanowires.

The photo-generated electrons from the dye can be injected into the ZnO photoanode and collected by the conductive substrate electrode. Besides the transport resistance of photoanode itself, such photoexcited carriers can also recombine with the excited dye. The finally collected electrons for photocurrent are the result of such competition between the transport and recombination. Single-crystal nanowires can provide more direct paths for electron transport from injection

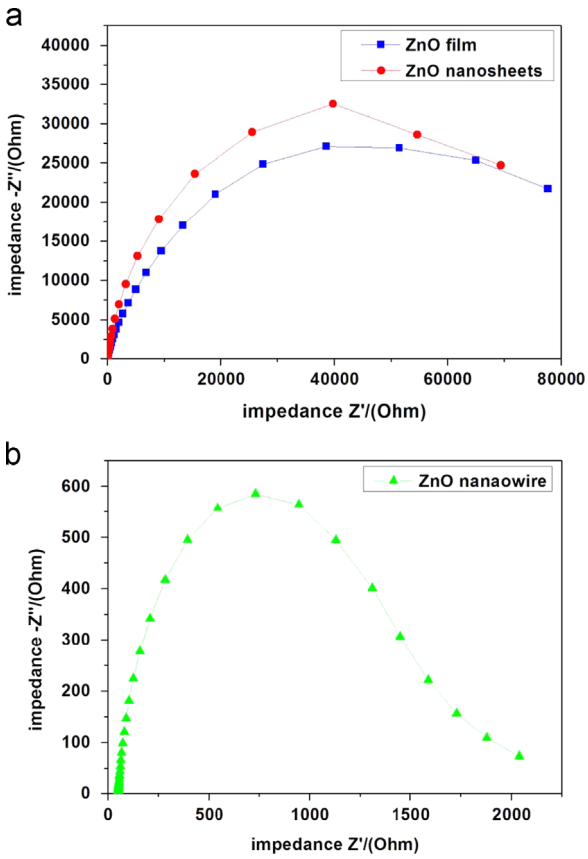

Fig. 5. EIS curves of different DSSC assembled with ZnO nanostructures.

to collection [33]. So the recombination reduced when photoelectrons injected into the nanowire photoanode. Compared with the ZnO film and nanosheet DSSCs, the scattering and trapping of the electrons at the photoanode grain boundaries reduce significantly and the opportunity of recombination between electron and excited dye is also smaller. Therefore, the ZnO nanowire-based DSSC shows smaller impedance and has bigger open-circuit voltage, which both enhances the photovoltaic efficiency.

4. Conclusions

In summary, ZnO nanowire, nanosheet, and film were grown with electrochemical deposition by just changing the concentration of the precursor solution. The formation of ZnO nanowire arrays was the result of the rapid growth along the (001)-direction for the *c*-axis oriented nuclei in thermodynamic equilibrium, while the ZnO film and nanosheets were the result of the growth in the non-equilibrium. The different types of ZnO nanostructures grown on conductive substrates were used as photoanodes for DSSCs. The photovoltaic performance of DSSCs showed that ZnO nanowire has a large specific surface area to absorb a large amount of dye. The enhanced scattering of nanowire arrays can improve the utilization of light and provide direct paths for the collection of photoexcited carriers. So the ZnO nanowires DSSC show the highest photoelectric conversion efficiency. However, the efficiency is still low, and

it has a long way for us to go to optimize the structure of ZnO photoanodes.

Acknowledgments

This work is supported by NSFC (51002065, 11174112) and Shandong Provincial Science Foundation for Disguised Youth Scholars (JQ201214). BC thanks the Taishan Scholar professorship tenured at University of Jinan (TSHW20091007) and the Program for New Century Excellent Talents in University (NCET-11-1027), Ministry of Education, China.

References

[1] Q. Zhang, C.S. Dandeneau, X. Zhou, G. Cao, ZnO nanostructures for dye-sensitized solar cells, Adv. Mater. 21 (2000) 1–22.
[2] B. O′Regan, M. Grätzel, A low-cost, high-efficiency solar cell based on dye-sensitized colloidal TiO_2 films, Nature 353 (1991) 737–740.
[3] Z.Y. Fan, H. Razavi, J.W. Do, Three-dimensional nanopillar-array photovoltaics on low-cost and flexible substrates, Nat. Mater. 8 (2009) 648–653.
[4] H.M. Wei, L. Chen, H.B. Gong, B.Q. Cao, Influence of ZnO nanorods morphology on the photovoltaic properties of ZnO/Cu_2O heterostructural solar cells, J. Inorg. Mater. 27 (2012) 833–837.
[5] H. Pan, N. Misra, S.H. Ko, C.P. Grigoropoulos, Melt-mediated coalescence of solution-deposited ZnO nanoparticles by excimer laser annealing for thin-film transistor fabrication, Appl. Phys. A 94 (2009) 111–115.
[6] H.M. Wei, H.B. Gong, B.Q. Cao, Three kinds of Cu_2O/ZnO heterostructure solar cells fabricated with electrochemical deposition and their structure-related photovoltaic properties, CrystEngComm 13 (2011) 6065–6070.
[7] Q. Zhang, C.S. Dandeneau, X. Zhou, G. Cao, ZnO nanostructures for dye-sensitized solar cells, Adv. Mater. 21 (2009) 4087–4108.
[8] G.M. Hua, Y. Zhang, J.X. Zhang, X.L. Cao, W. Xu, L.D. Zhang, Fabrication of ZnO nanowire arrays by cycle growth in surfactant-less aqueous solution and their on dye-sensitized solar cells, Mater. Lett. 62 (2008) 4109–4111.
[9] B.Q. Cao, W.P. Cai, Y. Li, Ultraviolet-light-emitting ZnO nanosheets prepared by a chemical bath deposition method, Nanotechnology 16 (2005) 1734–1738.
[10] L. Feng, A. Liu, M. Liu, Y. Ma, J. Wei, B. Man, Synthesis, characterization and optical properties of flower-like ZnO nanorods by non-catalytic thermal evaporation, J. Alloys Compd. 492 (2010) 427–432.
[11] H.T. Ng, J. Li, M.K. Smith, P. Nguyen, A. Cassell, J. Han, M. Meyyappan, Growth of epitaxial nanowires at the junctions of nanowalls, Science 300 (2003) 1249.
[12] Y.S. Lee, S.N. Lee, I.K. Park, Growth of ZnO hemispheres on silicon by a hydrothermal method, Ceram. Int. 39 (2013) 3043–3048.
[13] S.Y. Kim, M.C. Jeong, B.Y. Oh, W. Lee, J.M. Myoung, Fabrication of Zn/ZnO nanocables through thermal oxidation of Zn nanowires grown by RF magnetron sputtering, J. Cryst. Growth 90 (2006) 485–489.
[14] S.D. Shindea, G.E. Patila, D.D. Kajaleb, V.B. Gaikwada, G.H. Jain, Synthesis of ZnO nanorods by spray pyrolysis for H_2S gas sensor, J. Alloys Compd. 528 (2012) 109–114.
[15] C.Y. Tsay, M.C. Wang, Structural and optical studies on sol–gel derived ZnO thin films by excimer laser annealing, Ceram. Int. 39 (2013) 469–474.
[16] T. Terasako, Y. Ogura, K. Ohmae, S. Fujimoto, M. Yagi, S. Shirakata, Morphological, electrical and optical properties of highly oriented undoped and doped zinc oxide and cadmium oxide films grown by atmospheric-pressure chemical vapor deposition, Surf. Coat. Technol. 230 (2013) 245–253.
[17] J.Y. Yang, Y. Lin, Y.M. Meng, Y.H. Liu, A two-step route to synthesize highly oriented ZnO nanotube arrays, Ceram. Int. 38 (2012) 4555–4559.
[18] F.F. Wang, R.B. Liu, A.L. Pan, The optical properties of ZnO sheets electrodeposited on ITO glass, Mater. Lett. 61 (2007) 2000–2003.
[19] Q.F. Zhang, C.S. Dandeneau, X.Y. Zhou, G.Z. Cao., ZnO nanostructures for dye-sensitized solar cells, Adv. Mater. 21 (2009) 4087–4108.
[20] Y.F. Hsu, Y.Y. Xi, A.B. Djurisic, W.K. Chan, ZnO nanorods for solar cells: hydrothermal growth versus vapor deposition, Appl. Phys. Lett. 92 (2008) 1335071–1335073.
[21] Y.M. Meng, Y. Lin, Y.B. Lin, Electrodeposition for the synthesis of ZnO nanorods modified by surface attachment with ZnO nanoparticles and their dye-sensitized solar cell applications, Ceram. Int. 40 (2014) 1693–1698.
[22] M. Zhu, L. Chen, H.B. Gong, M. Zi, B.Q. Cao, A novel TiO_2 nanorod/na noparticle composite architecture to improve the performance of dye-sensitized solar cells, Ceram. Int. 40 (2014) 2337–2342.
[23] J.C. Sin, S.M. Lam, K.T. Lee, A.R. Mohamed, Preparation and photocatalytic properties of visible light-driven samarium-doped ZnO nanorods, Ceram. Int. 39 (2013) 5833–5843.
[24] X.J. Qin, G.J. Shao, L. Zhao, The effect of surfactant on the structure and properties of ZnO films prepared by electrodeposition, Mater. Sci. Eng. B 177 (2012) 1678–1681.
[25] Y.P. Sheng, Y. Jiang, X.Z. Lan, C. Wang, S.Y. Li, X.M. Liu, H.H. Zhong, Mechanism and growth of flexible ZnO nanostructure arrays in a facile controlled way, J. Nanomater. 2011 (2011) 1–13.
[26] Y.F. Hao, G.W. Meng, C.H. Ye, X.R. Zhang, L.D. Zhang, Kinetics-driven growth of orthogonally branched single-crystalline magnesium oxide nanostructures, J. Phys. Chem. B 109 (2005) 11024–11208.
[27] Y.F. Hao, G.W. Meng, Z.L. Wang, C.H. Ye, L.D. Zhang, Periodically twinned nanowires and polytypic nanobelts of ZnS: the role of mass diffusion in vapor − liquid − solid growth, Nano Lett. 6 (2006) 1650–1655.
[28] B. Illy, B.A. Shollock, J.L. M-Driscoll, M.P. Ryan, Electrochemical growth of ZnO nanoplates, Nanotechnology 16 (2005) 320–324.
[29] K. Zarebska, M. Kwiatkowski, M. Gniadek, M. Skompska, Electrodeposition of $Zn(OH)_2$, ZnO thin films and nanosheet-like Zn seed layers and influence of their morphology on the growth of ZnO nanorods, Electrochim. Acta 98 (2013) 255–262.
[30] B.Q. Cao, W.P. Cai, Y. Li, F.Q. Sun, L.D. Zhang, Ultraviolet-light-emitting ZnO nanosheets prepared by a chemical bath deposition method, Nanotechnology 16 (2005) 1734–1738.
[31] Y.F. Hao, G.W. Meng, Y. Zhou, M.G. Kong, Q. Wei, M. Ye, L. D. Zhang, Tuning the architecture of MgO nanostructures by chemical vapour transport and condensation, Nanotechnology 17 (2006) 5006–5012.
[32] J.B. Han, F.R. Fan, C. Xu, S.S. Lin, M. Wei, X. Duan, Z.L. Wang, ZnO nanotube-based dye-sensitized solar cell and its application in self-powered devices, Nanotechnology 21 (2010) 4052031–40520317.
[33] L. Vayssieres, Growth of arrayed nanorods and nanowires of ZnO from aqueous solutions, Adv. Mater. 15 (2003) 464–466.